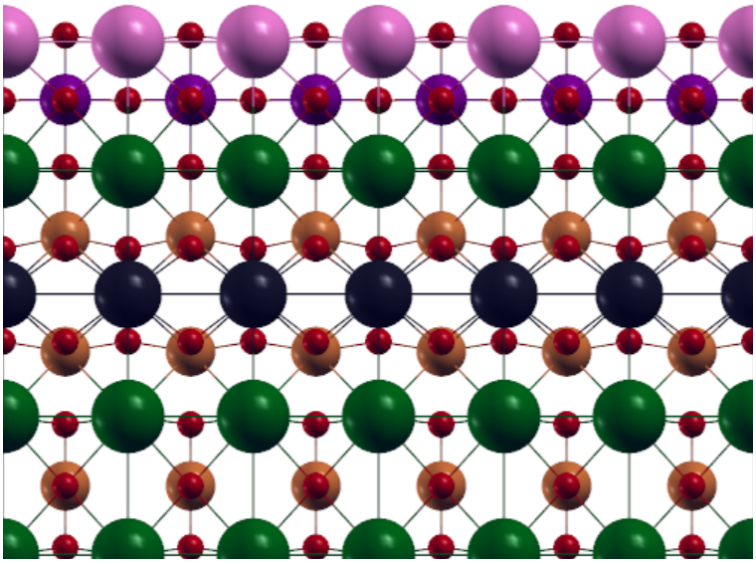

Characterisation of YBCO surfaces and STO/YBCO interfaces using DFT

Master's thesis in Nanotechnology

ERIKA DANIELSSON

DEPARTMENT OF MICROTECHNOLOGY AND NANOSCIENCE (MC2)

CHALMERS UNIVERSITY OF TECHNOLOGY
Gothenburg, Sweden 2024
www.chalmers.se

MASTER'S THESIS 2024

Characterisation of YBCO surfaces and STO/YBCO interfaces using DFT

ERIKA DANIELSSON

CHALMERS
UNIVERSITY OF TECHNOLOGY

Department of Microtechnology and Nanoscience (MC2)
Quantum Device Physics Laboratory
CHALMERS UNIVERSITY OF TECHNOLOGY
Gothenburg, Sweden 2024

Characterisation of YBCO surfaces and STO/YBCO interfaces using DFT
ERIKA DANIELSSON

Supervisor and examiner:
Elsebeth Schröder
Department of Microtechnology and Nanoscience (MC2)

Master's Thesis 2024
Department of Microtechnology and Nanoscience (MC2)
Quantum Device Physics Laboratory
Chalmers University of Technology
SE-412 96 Gothenburg
Telephone +46 31 772 1000

Cover: Side view of an optimised STO/YBCO interface.

Typeset in LaTeX
Printed by Chalmers Reproservice
Gothenburg, Sweden 2024

Characterisation of YBCO surfaces and STO/YBCO interfaces using DFT
ERIKA DANIELSSON
Department of Microtechnology and Nanoscience (MC2)
Chalmers University of Technology

Abstract

The focus of this project was to investigate the surface structure of the high temperature superconductor $YBa_2Cu_3O_7$ (YBCO) as well as determining the interface structure when YBCO is capped with a thin film of $SrTiO_3$ (STO). The motivation for STO capping is to see if it can protect YBCO from degradation losing its superconductivity. Here surface and interface terminations were studied with a literature review as well as calculations based on density functional theory (DFT). Together with this, a method of determining the surface energy contribution of a slab structure was used which found the CuO_2(Y) surface and the BaO(CuO) surface as most probable surface terminations of YBCO. The change in electron density was also studied that showed a rearrangement of charges at the interface in the STO/YBCO systems. The STO capping itself together with electronic redistribution at the interface made the top YBCO layers become more bulk-like, and this can be a part of the explanation how STO can protect the YBCO surface.

Keywords: Density functional theory, Yttrium barium copper oxide, Strontium titanium oxide, Surface energy, Asymmetric slab, Electron density.

Acknowledgements

My biggest thanks go to my supervisor and examiner Elsebeth Schröder. You have really helped and supported me throughout this project. From finding a topic to completing the report, for all the guidance and for always being helpful and encouraging. It has indeed been a great help to me. I would also like to thank Alexei Kalaboukhov for letting me take part of your unpublished results which are the basis of this project. Lastly, I want to acknowledge Chalmers e-Commons at Chalmers (C3SE) which provided the resources that enabled the computations.

Erika Danielsson, Gothenburg, August 2024

List of Acronyms and Elements

Below is the list of acronyms that have been used throughout this thesis listed in alphabetical order:

DFT	Density functional theory
HTS	High-temperature superconductor
PLD	Pulsed laser deposition
PP	Pseudopotential
SCF	Self-consistent field
STO	Strontium titanium oxide, $SrTiO_3$
STO/YBCO	Interface of STO onto YBCO with YBCO lattice constants
TEM	Transmission electron microscopy
vdW-DF-cx	van der Waals consistent exchange density functional
XPS	X-ray photoelectron spectroscopy
YBCO	Yttrium barium copper oxide, $YBa_2Cu_3O_7$
YBCO/STO	Interface of YBCO onto STO with STO lattice constants

Elements

The atomic colors that was used in the figures for this thesis are illustrated below:

- Barium (Ba)
- Copper (Cu)
- Oxygen (O)
- Strontium (Sr)
- Titanium (Ti)
- Yttrium (Y)

Contents

1
Introduction

The discovery of superconducting materials in the early twentieth century, opened a new research area, important for basic research and applications. Under a certain temperature, the critical temperature, the resistivity of such material vanished resulting in a conducting material without energy (or heat) losses. In the 80's, the first superconducting materials with critical temperatures above 80 K were found. These materials were crystal structures consisting of copper oxides.

Yttrium barium copper oxide (YBCO) is one high-temperature cuprate superconductor. Much effort has been put on choosing substrate on which YBCO can be grown to achieve high quality films. Another aspect of YBCO as a functional material, is to protect it from degradation in applications. One way is simply to grow a thin layer of another material onto YBCO to protect the superconducting properties.

A complement, or replacement, for experiments is computing modelling and simulations. How calculations can be used depend on the situation. Sometimes the studied system is too large and complex to study experimentally, or if one part of a system needs to be developed or designed, it can be easier to limit the system. The physical system can also have too much uncertainty to trust results. To study material behaviour on atomic or electronic scale, computations are helpful and sometimes necessary. One method to perform calculations on atomic systems is to use the quantum mechanical based density functional theory (DFT).

Strontium titanium oxide (STO) is one material suggested to protect the superconductivity. From this, the objective of this project is to gather insights of the interface between YBCO and a thin film of STO. The work is based on computations, to be a complement to ongoing research. A literature review on YBCO surfaces and interfaces of STO and YBCO is also provided. Atomic structures will be analysed by measuring distances between atomic planes in the YBCO crystal and electronic properties by studying the change in electron densities for interface structures. Also a method of calculating the surface energy of asymmetric slab will be used to compare the stability of different YBCO surfaces.

2
Theory

This chapter gives some background on the high-temperature superconducting material YBCO and the degradation problematic, resulting in loss of superconductivity. Further, the semiconducting material STO will be introduced, and the structural similarities with YBCO is studied. A short introduction to the theory used for the calculations in this work is also given.

2.1 YBCO and high temperature superconductors

Cuprate superconductors are crystalline materials consisting of copper oxide layers and metallic ions. The structure consists of three perovskite-like unit cells that are vertically stacked. In these structures, the electrons in the CuO_2-planes interact by moving between the Cu atoms. These electrons between the Cu-O bonds in the crystal create the superconductivity of the material, described in Ref. [1]. Yttrium barium copper oxide (YBCO) is one such material and is the first known high temperature superconductor (HTS) with a critical temperature above 77 K [2], the boiling point of nitrogen. The general formula is $YBa_2Cu_2O_{7-x}$ depending on the oxygen doping level, $x \in [0, 1]$.

The chemical formula of the fully oxygen doped $YBa_2Cu_3O_{7-x}$ is $YBa_2Cu_3O_7$, with x = 0, and is further referred to as YBCO. YBCO has an orthorhombic unit cell, with lattice parameters $a \neq b \neq c$, shown in Figure 2.1a. The cell consists of 13 atoms in six atomic layers in the c direction, also labeled in the figure. In the center of the unit cell an Y^{3+} ion is located, surrounded by two CuO_2 planes with net charge -2. The bulk structure is symmetric around the centered Y atom, the next planes after the CuO_2-Y-CuO_2 structure are an uncharged BaO plane on each side, and the outermost a plane of CuO chains, with net charge +1, in the b direction. In Figure 2.1b, the unit cell is viewed in the ac and bc plane with all O atoms from neighbouring unit cells included. The blue regions represent the Cu-O bonds in between where the superconducting electrons are exchanged.

Since the structure of YBCO, and other HTSs, is complex, there have been much research on physical and electronic properties of the materials [3]. Also fabrication techniques as well as applications are important for YBCO research. For superconducting applications HTSs are important due to operation temperature and cooling costs compared to low-temperature superconductors. Examples of applications are magnets and in Josephson junctions and superconducting quantum interference devices (SQUIDs) [4].

2.2 STO

Strontium titanium oxide (STO) with chemical formula $SrTiO_3$ is a perovskite structured indirect bandgap semiconductor consisting of Sr^{2+}, Ti^{4+} and O^{2-} ions. The primitive, cubic unit cell

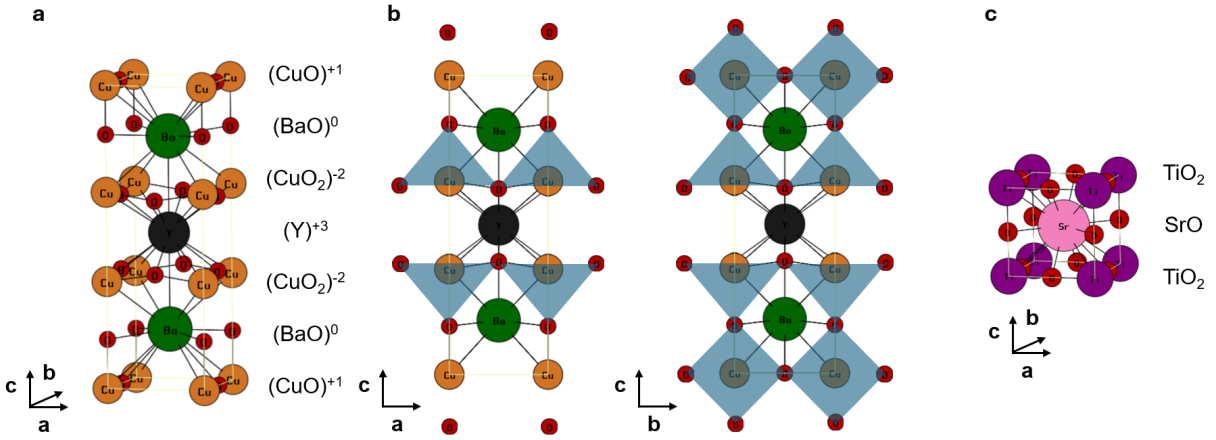

Figure 2.1: Schematic unit cell of YBCO (**a**) and STO (**c**) including repeated atoms from neighbouring unit cells. The atomic planes are labeled. The blue shaded areas in the 2D representations (**b**) show the the Cu-O bonds for all the Cu atoms in the unit cell.

consists of five atoms of alternating and uncharged SrO and TiO_2 layers, see Figure 2.1c. The material is often used as substrate for microelectronic devices. The unit cell of STO is in many ways similar to the one of YBCO since YBCO in principle consists of three vertically stacked perovskite structures. STO is also usually used as substrate for YBCO due to the similar lattice constants of the two materials [5].

2.3 Degradation of YBCO

To study and use YBCO for different applications high quality structures such as thin films are needed [6]. It has been showed that YBCO is very sensitive to water and air, negatively affecting the superconducting phase of YBCO. Conclusions from experiments in Ref. [7] show that trivalent Cu ions of YBCO (in the CuO chains) are reduced in the presence of water, with products such as $BaCO_3$, CuO and Y_2BaCuO_5. Flux avalanche of superconducting films also negatively affects the superconductivity. In general there are two ways of protecting superconductors from degradation according to Ref. [8]: To protect the surface with another material or to dope the structure to reduce the reactivity with water and air. Metal coatings can, for instance, reduce the flux avalanches of YBCO films, obtained in Ref. [9]. Also measurements with STO as insulating layer have been made for YBCO in SQUID applications, see Ref. [10].

There is current research on YBCO films capped with a nm-thin STO layer, Ref. [11]. For the experiments a 10 nm thick layer YBCO-film was grown using pulsed laser deposition (PLD) onto a MgO substrate on which a thin film of STO is sputtered. From X-ray photoelectron spectroscopy (XPS) it was shown that STO capping decreased the amount of both Cu and Y in the signal. For Ba, there was another trend. Without capping, XPS indicated both Ba and $BaCO_3$, but with a thin layer of STO the Ba oxide signal was not present, and the Ba peak was not suppressed. Since $BaCO_3$ is one of the reported, Ref. [7], products from YBCO reaction with water, the results show that STO can protect YBCO from degradation. How and why the presence of STO changes the chemical composition is yet unclear and will be further studied in this work, from a theoretical approach.

2.4 Density functional theory

The calculations performed in this project are based on density functional theory (DFT). This theory is based on quantum mechanics describing molecular and bulk systems. By solving the Schrödinger equation the ground state energy and optimal atomic positions can be determined for a specific system. One important step of the DFT is to use a charge density defined as the probability of finding an electron in a volume element, instead of solving for the quantum wave function of the system [12].

In general, it is hard to exactly solve for multi-body systems, since it would be very complex and time consuming. Instead there are several approximations to simplify the DFT calculations. One example is to use pseudopotentials (PP) which are effective potentials instead of the real electron potentials. The PPs are designed from atomic calculations [12]. Different types of PPs work differently well for different atomic systems and also the PP must work for each element in that system. The choice of PP also results in different total energies for the system, because the energy has different zero points. Still, the energy differences within the system remain constant.

2.4.1 Calculation process

The princple of a DFT calculation is to find the total energy from an input atomic structure with iterative self-consistent calculations [12]. This is illustrated in Figure 2.2 where also the process of a relaxation calculation is presented. For a SCF calculation, the first step is to calculate the electron density $n_0(r)$ from the atomic coordinates and other input parameters as PPs. From that an effective potential is calculated, that further can be used to solve the independent one-electron equations. Together with an approximation for the exchange-correlation potential, a new electron density $n(r)$ is calculated. When the guessed and the calculated electron density converge, the ground state energy E_0 of the system is found and the SCF calculation is done.

For relaxation calculations where the atomic positions are also optimised, there is an additional iteration process to find the optimal geometry of the studied system. By knowing the

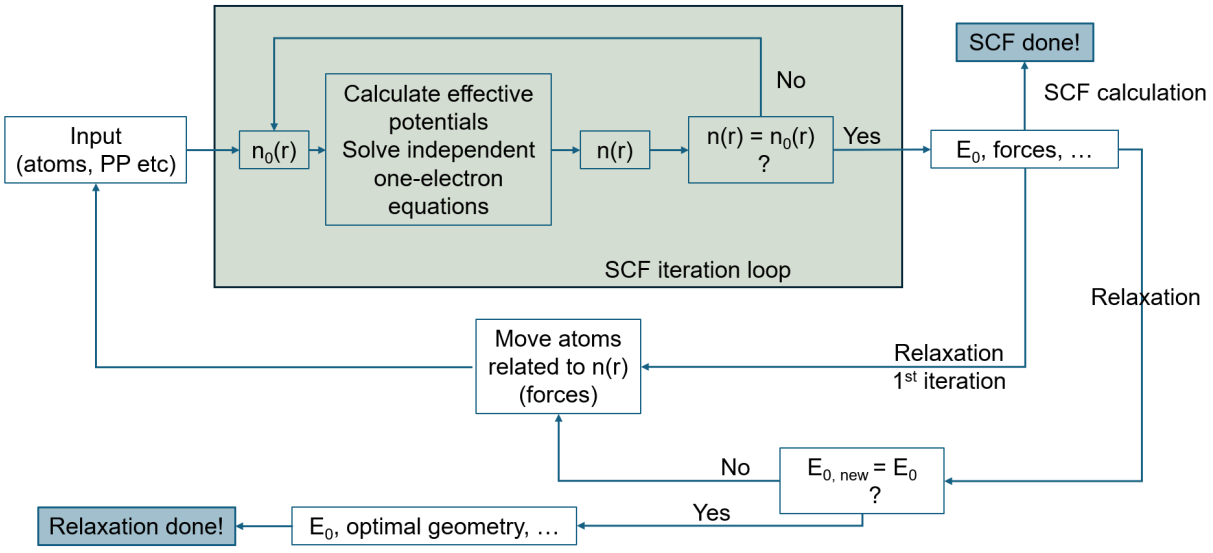

Figure 2.2: Simplified flowchart of the steps in a SCF and relaxation calculation based on DFT.

charge density from the SCF calculation it is possible to calculate the forces on the atoms. In a relaxation the forces are used to slightly move the atoms to more favorable positions. From the new positions a new SCF iteration loop is made, resulting in another ground state energy. The relaxation calculation is finished when the energy and geometry has converged.

3
Methods

In this chapter, the methods of the computations are introduced, as well as the analysis methods of the calculations. The calculations of crystals structures were performed using Quantum ESPRESSO [13, 14, 15], an open source DFT computer code. Quantum ESPRESSO can optimise atomic and electronic structures of different materials using pseudopotentials (PP). After the input parameters to Quantum ESPRESSO are presented, the bulk, surface, and interface calculations are explained. The last part of this chapter derives how the surface energy of an asymmetric slab can be calculated, and the principle of analysing differences in electron density.

3.1 Calculation details

In total three types of calculations were performed: For geometry optimisation of bulk materials a variable-cell relaxation was used, for surface slabs a relaxation of the atomic positions was used together with a dipole correction, and for already optimised structures only a self-consistent field (SCF) calculation was made. The calculations were carried out at vacuum and 0 K and the visualisations of both atomic structures and electron densities is performed in XCrySDen [16], a visualisation program for crystalline and molecular materials. For the calculations, the van der Waals consistent exchange density functional (vdW-DF-cx) was used [17, 18]. Kinetic energy cutoff for wave functions were set to 60 Ry and cutoff for charge density to 480 Ry which is above the recommended minimum values for the used PPs.

The k points used were automatically generated on a uniform grid. For YBCO bulk, the number of k points were set to $20 \times 20 \times 6$, and for cubic STO $20 \times 20 \times 20$ due to the tetragonal and cubic structures of YBCO and STO, respectively. Higher number of k points increases the accuracy of the calculations, but also the computation time. Due to the time limit of this project the k points for relaxation and SCF calculations performed of surface and interface structures were set to $6 \times 6 \times 1$. Convergence threshold for electronic self-consistency was $n \cdot 10^{-8}$ (a.u.) and convergence thresholds for forces and total energy for ionic minimisation were set to $1 \cdot 10^{-4}$ (a.u.) and $n \cdot 10^{-6}$ (a.u.), respectively, where n is the number of atoms in the calculated system.

3.2 Pseudopotentials

The pseudopotentials (PP) used during the calculations was taken from the PSlibrary package 1.0.0 [19]. Initially PBEsol potentials were used, but there was problem with convergence of the SCF calculations, especially for the slab optimisations where a dipole correction was necessary. Which of the atoms the PBEsol potentials did not work for, could not be investigated due to the time limit of the project. Instead, another type of PPs were used: PBE potentials, that successfully converged the performed DFT calculations.

3.3 Bulk optimisation of YBCO and STO

The first calculations were to determine the bulk structures of YBCO and STO, separately. The input structures were taken from Materials Project [5], a database of computed properties of inorganic materials, for $Ba_2YCu_3O_7$ (mp-20674) and $SrTiO_3$ (mp-5229) from database version v2023.11.1. YBCO has an orthorhombic, and STO a cubic structure, and the cell parameters and atomic positions were optimised in Quantum ESPRESSO using a variable-cell relaxation calculation.

3.4 Slab optimisation of YBCO and STO surfaces

To optimise surface structures of YBCO and YBCO covered with STO, slab calculations were performed. A slab is an extended unit cell were vacuum is added above the crystal to keep the periodically repeated slabs sufficiently apart (in the c direction), and to include surface effects and enable surface relaxations. The vacuum thickness was set to 15 Å. As input to the YBCO surface slab calculations, the optimised bulk structure of YBCO was used. In the c direction, there are six possible surface terminations of YBCO, by the assumption that the bulk has no reconstructions. Slabs of two unit cells, with thickness of 23 Å, or twelve atomic layers, were constructed. The six bottom layers were fixed (i.e. forces on atoms were set to 0) to keep them in the bulk structure while the six top layers were allowed to relax due to surface properties.

The calculations are periodically repeated, also in the c direction. Thus, a dipole correction needs to be considered. In general, adjustment of the dipole is necessary for asymmetric systems, as slab unit cells. If not, the dipole in one slab will interact with neighbouring slabs above and below throughout the calculation process, resulting in an artificial dipole. The position where the dipole potential was adjusted was set in the center of the vacuum region, i.e., 7.5 Å above the surface. The potential decreased back to 0 in a region of $0.005 \cdot c_{cell}$ Å, where c_{cell} is the total height of the slab, vacuum included. Figure 3.1 illustrates the principle of the performed slab calculations.

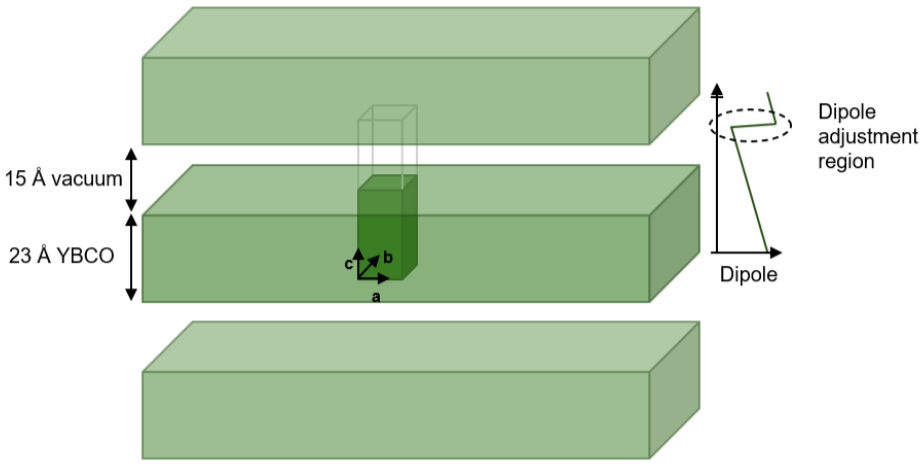

Figure 3.1: Schematic illustration the YBCO unit slab used for the calculations including the periodically repeated slabs in the a, b and c directions. The principle of dipole correction in the c direction is also visualised.

Since the aim of this thesis is to find out more about the characteristics of STO capped YBCO, the last step of the calculations is to study the interface structures. The geometry optimisation of an interface structure is based on an optimised YBCO surface with added STO layers onto. Initially, one unit cell of STO (five atoms in two layers) is added onto YBCO slightly strained to fit the size of the a and b parameters of YBCO. This system is in this thesis labeled a STO/YBCO interface. For one of the STO/YBCO interfaces, an additional layer of STO was added onto the optimised interface, and finally a third layer, as if STO was grown onto the YBCO surface layer by layer.

3.5 Analysis of surfaces and interfaces

Besides the optimisation of the YBCO surfaces and YBCO/STO interfaces, a comparison with surface terminations obtained in the literature was done. The review was also used to choose which interface structures to optimise and analyse further. The calculated YBCO surfaces were also further studied by comparing atomic positions with bulk YBCO. The stability of the different surface terminations was studied by calculating the surface energies, described below.

3.5.1 Calculation of surface energies

One method of calculating the surface energies of asymmetric slabs was suggested by Ref. [20]. A slab has two surfaces, here denoted A and B. All atoms in the slab are assumed to contribute to one of the both surfaces: The atoms in the upper half belong to surface A and the atoms in the lower half belong to surface B. To extract the surface energy of a relaxed surface, four slab energies E^{slab} are needed: One with both the surface layers A and bottom layers B fixed, one with A relaxed and B fixed, one with A fixed and B relaxed, and one with both A and B atoms relaxed. These slab energies are compared to the corresponding bulk value ηE^{bulk}, where η is the number of unit cells, and weighted by the surface area A:

$$\varepsilon_i = \frac{E_i^{slab} - \eta E^{bulk}}{A} \tag{3.1}$$

$\varepsilon_i, i = 1, 2, 3, 4$ denotes the four weighted slab energies. The slab energies can also be described as the sum of the surface energy contribution E from the top surface atomic layers A and bottom atomic layers B:

$$\begin{cases} E_A^f + E_B^f = \varepsilon_1 \\ E_A^r + E_B^f = \varepsilon_2 \\ E_A^f + E_B^r = \varepsilon_3 \\ E_A^r + E_B^r = \varepsilon_4 \end{cases} \tag{3.2}$$

The indices f and r correspond to fixed or relaxed surface atoms during the optimisation calculations. The four equations in Eq. (3.2) can, with matrix representation, be written on the form $\hat{A}\vec{E} = \vec{\varepsilon}$:

$$\begin{pmatrix} 1 & 1 & 0 & 0 \\ 0 & 1 & 1 & 0 \\ 1 & 0 & 0 & 1 \\ 0 & 0 & 1 & 1 \end{pmatrix} \begin{pmatrix} E_A^f \\ E_B^f \\ E_A^r \\ E_B^r \end{pmatrix} = \begin{pmatrix} \varepsilon_1 \\ \varepsilon_2 \\ \varepsilon_3 \\ \varepsilon_4 \end{pmatrix} \tag{3.3}$$

The solution vector $\vec{E}$ cannot be determined exactly, but a numerical solution can be found by minimising the sum of the squared relative differences of each row i:

$$\sum_i \left(\frac{\vec{\varepsilon_i} - (\hat{A}\vec{x})_i}{\vec{\varepsilon_i}} \right)^2 \tag{3.4}$$

As initial guess for the solution is $E_A^f = E_B^f = \varepsilon_1/2$ and $E_A^r = E_B^r = \varepsilon_4/2$, physically meaning surface layers A and B have equal influence of the frozen and fully relaxed slab, respectively. This method is by Ref. [20] called the simultaneous equations method. For YBCO surfaces with slabs of two unit cells with 12 atomic layers, and $\eta = 2$, the six top layers will be included in surface A, and the six bottom layers in surface B.

3.5.2 Electron densities

For one of the interface structures, an analysis was carried out of how the charge density, or more specific, the electron density, changed when STO was added onto YBCO compared to when the materials are in separated systems. This was made for different capping thickness of STO, but the number of charge analysis calculations with different of STO capping thickness were restricted by the time restraint of this project.

The change in electron density $\Delta n_{AB}(r)$ (in units of charge per unit volume) for an integrated structure AB of two different materials compared to the materials separated, A and B, is described as:

$$\Delta n_{AB}(r) = n_{AB}(r) - n_A(r) - n_B(r) \tag{3.5}$$

Thus, three SCF calculations of the interface structures were made: One for the complete interface $n_{AB}(r)$, one without the YBCO atoms $n_A(r)$ and the third without the STO atoms $n_B(r)$. The atomic positions of the two last calculations were kept unchanged compared to the complete interface structure. By post-processing the data of charges from the SCF calculation in Quantum ESPRESSO, the difference of the electron densities could be analysed.

4

Results and discussion

In this chapter, the results of the calculations are presented and discussed. Included is also a literature review of YBCO surfaces and interface structures of YBCO and STO. The first presented calculation part is the unit cell optimisation of YBCO and STO followed by an analysis of the different YBCO surfaces comparing atomic distances and surface energies. Thereafter, a discussion of possible STO/YBCO interfaces and calculations of some of the interfaces is made. The chosen interfaces are also analysed further for different STO capping thicknesses by studying the difference in electron density.

4.1 Bulk structures of YBCO and STO

The optimised bulk structures for YBCO and STO are shown in Figure 4.1. The calculated lattice parameters for YBCO are a = 3.80 Å, b = 3.88 Å and c = 11.52 Å, and for STO is a = 3.90 Å. The input parameters from Materials Project [5] are slightly bigger with a = 3.84 Å, b = 3.93 Å, c = 11.82 Å for YBCO and a = 3.91 Å for STO. One difference between the Materials Project results and the calculations presented here, is that dispersion is included in the calculations (in the vdW-DF-cx). For a layer structured material as YBCO, this gives a more realistic and stronger binding between the layers, resulting in a smaller c parameter.

The calculated lattice parameter of STO is 0.6% and 2.7% larger than the a and b parameters in YBCO, respectively. This means that the lattice parameters of YBCO and STO match each other well. As a result, if STO is added onto a YBCO surface the STO unit cell is slightly compressed in the a and b directions. The unit cell visualisation in Figure 4.1 indicates that

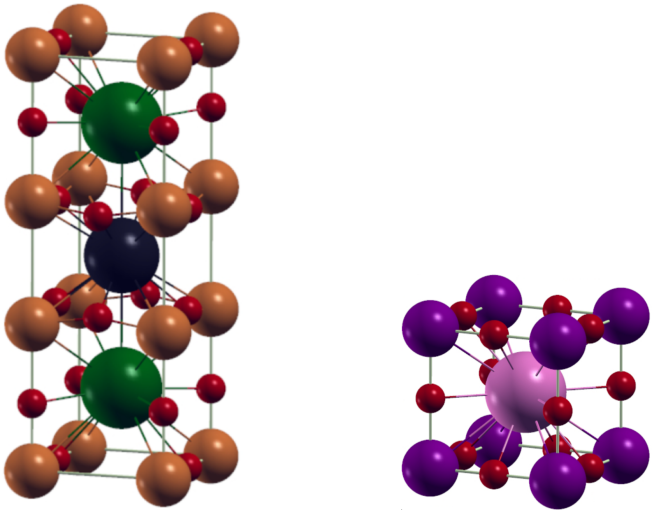

Figure 4.1: Visualisation of optimised bulk structures for YBCO and STO.

three vertically stacked STO unit cells also match the c parameter of YBCO. More specific, three STO unit cells are only 1.6% larger than one YBCO unit cell.

4.2 Surface termination of YBCO

Both experiments and theoretical research have spend much time on studying the surface termination of YBCO. There are six possible ideal surface terminations of YBCO in the c direction presented in Table 4.1, for slabs with twelve layers. The last three rows in Table 4.1 show which surface termination is found in different references, and also YBCO interface termination for interfaces between YBCO and STO. The interesting interface in this project is the STO/YBCO interface where STO is added onto YBCO with lattice parameters of YBCO. However, also the opposite case where YBCO is grown onto STO is included in Table 4.1. The interface structures are further discussed in section 4.3.

From a surface stability perspective an initial hypothesis is that BaO would be a promising YBCO surface since BaO is the only YBCO layer that is uncharged. As can be seen in Table 4.1, there are no simple answers of what the YBCO surface looks like, which is also concluded in Ref. [23]. The results depend on contamination from the environment, how the surface is prepared and how the surface termination is measured. It also depends on the studied sample, if the surface occurs from cleaving the YBCO crystal or as top layer of growing a thin film.

In a review of YBCO surfaces, Ref. [23], a discussion of all possible surface terminations is made. From the view of bond strengths between the YBCO atomic layers and crystal cleavage, the CuO_2(Y) and BaO(CuO) surface terminations are more probable than the BaO(CuO_2) and CuO(BaO) surfaces. The CuO_2(Y) surface, for instance, means CuO_2 is the surface layer of YBCO, and Y as the first sublayer. The reason to the conclusions is that the Cu-O bond length

Table 4.1: Possible surface terminations of YBCO in the c direction with following sublayers for two unit cell thick slabs. Included is also references discussing surface and interface terminations of YBCO and STO.

Surface layer	CuO	BaO	CuO_2	Y	CuO_2	BaO
Sublayer 1	BaO	CuO_2	Y	CuO_2	BaO	CuO
2	CuO_2	Y	CuO_2	BaO	CuO	BaO
3	Y	CuO_2	BaO	CuO	BaO	CuO_2
4	CuO_2	BaO	CuO	BaO	CuO_2	Y
5	BaO	CuO	BaO	CuO_2	Y	CuO_2
⋮	⋮	⋮	⋮	⋮	⋮	⋮
11	BaO	CuO	BaO	CuO_2	Y	CuO_2
References						
Uncapped YBCO	[3, 21]	[3, 22]	[23]		[22]	[22, 23]
YBCO/STO interface		[6, 21, 24]			[6]	[24]
STO/YBCO interface		[21]				

in the c direction is shorter, and thus stronger, between the CuO and BaO layers in the YBCO crystal. This fact is valid also for the calculations in this thesis where the vertical Cu-O bonds are 0.16 Å and 0.19 Å.

The two last possible cleavages of the YBCO crystal are between the Y and CuO_2 planes. From the discussions of Ref. [3] and Ref. [23] this will not be probable due to strong bonds and a large electrostatic instability if the positive Y ion is not compensated by the CuO_2 planes. This is true for the Y(CuO_2) surface, but also the CuO_2(BaO) surface. However, the angle-resolved photoemission spectroscopy (ARPES) study, Ref. [3], found the most probable cleavage between the YBCO layers (in the c direction) would appear between the CuO and BaO layers. Their reasoning is that the CuO_2-Y-CuO_2 center of the unit cell, also attract the BaO layers. Since the CuO layers are most distanced to the Y ion, the cleavage of the YBCO unit cell occur between the CuO and BaO layers, resulting in the CuO(BaO) surface and BaO(CuO_2) surface.

From an experimental perspective, the surface termination of YBCO surfaces not always can be explained by the principles of bond strengths and YBCO crystal cleaving. If YBCO instead is grown as a thin film, other surface terminations of YBCO also is found, depending on the substrate, how the film is prepared and the environment. Transmission electron microscopy (TEM) of PLD grown YBCO onto a STO substrate also concludes that the surface termination of YBCO is a CuO layer [21]. The discussion is founded in the fact that the top STO substrate layer is TiO_2 and that the first STO layer consists of BaO, followed by a CuO_2 layer. The YBCO growth will continue until a complete number of unit cells is reached, resulting in a CuO surface layer.

Another experiment of epitaxial grown YBCO films shows from XPS that the surface termination depends on the annealing temperature [22]. The BaO(CuO) surface dominated at a low annealing temperature, increasing the temperature resulted in a CuO_2(BaO) surface, and for strong annealing the BaO(CuO_2) was present. Other aspects to consider are that measurements of YBCO surfaces also indicate other surface terminations than the ideal YBCO stacking sequence. A common case is loss of oxygen at the surface [23]. The XPS signals of the YBCO films in Ref. [22] also found a $BaCuO_2$ phase at the surface which origins from either a new surface compound or a reconstructed surface atom composition of the ideal YBCO structure.

4.2.1 Atomic distances in the YBCO surface slabs

The difference between a slab and a bulk structure is that atoms close to the vacuum might move compared to the bulk case. A comparison of the atomic distances (Å) in the optimised YBCO slab structures is presented in Table 4.1. The measured distances, between the Y, Ba and C atoms, are also indicated in the bulk unit cell in the Table 4.2. Since the slabs consist of twelve layers with the six bottom layers fixed in the bulk structure, the last measured distance given in Table 4.2 for each slab is the distance between the lowest relaxed layer and the top fixed atomic layer. The percentage change of the two deepest measured distances from the slab surface compared to bulk is below 0.5 % for all surface terminations. That mean six relaxed atomic layers are enough to simulate a surface relaxation of YBCO.

For the optimised surfaces, the largest change in distance occurs between the top layers where the outermost YBCO layer is compressed, except for the case of the CuO_2(BaO) terminated surface. There, the distance between the two top layers is stretched out compared to bulk YBCO.

Table 4.2: Atomic distance (Å) and relative change compared to corresponding bulk value between neighboring Cu, Ba and Y atoms for the six YBCO surface terminations. The measured distances are marked in the unit cell.

Surface / Atomic distance		CuO (BaO)	BaO (CuO_2)	CuO_2 (Y)	Y (CuO_2)	CuO_2 (BaO)	BaO (CuO)
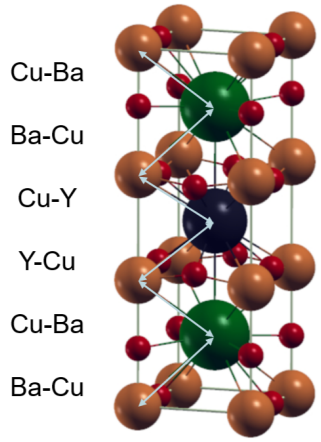	Cu-Ba	3.35 (-2.3%)					
	Ba-Cu	3.37 (+0.5%)	3.29 (-2.0%)				
	Cu-Y	3.20 (-0.2%)	3.25 (+1.6%)	3.16 (-1.4%)			
	Y-Cu	3.20 (+0.0%)	3.20 (+0.1%)	3.26 (+1.7%)	3.12 (-2.6%)		
	Cu-Ba	3.36 (+0.1%)	3.36 (+0.1%)	3.33 (-0.6%)	3.42 (+2.1%)	3.53 (+5.2%)	
	Ba-Cu	3.43 (+0.1%)	3.43 (+0.1%)	3.44 (+0.6%)	3.34 (-2.6%)	3.57 (+4.3%)	3.32 (-3.2%)
	Cu-Ba		3.43 (+0.0%)	3.43 (+0.0%)	3.47 (+1.3%)	3.42 (-0.2%)	3.48 (+1.6%)
	Ba-Cu			3.37 (+0.4%)	3.35 (+0.0%)	3.37 (+0.3%)	3.35 (-0.1%)
	Cu-Y				3.19 (-0.3%)	3.21 (+0.3%)	3.19 (-0.2%)
	Y-Cu					3.21 (+0.3%)	3.20 (-0.1%)
	Cu-Ba						3.37 (+0.3%)

Simultaneously, as the distance between the outermost layers decreases, the second distance from the surface of the slab increases, in practice meaning that the first sublayer moves closer to the surface. This is illustrated in Figure 4.2 for the $BaO(CuO_2)$ surface where side view images of the optimised surface and bulk structures are placed onto each other. The movement of atoms compared to bulk structure is showed as blur. The explanation is that the sublayer compensates the lack of shared electrons for the surface layer.

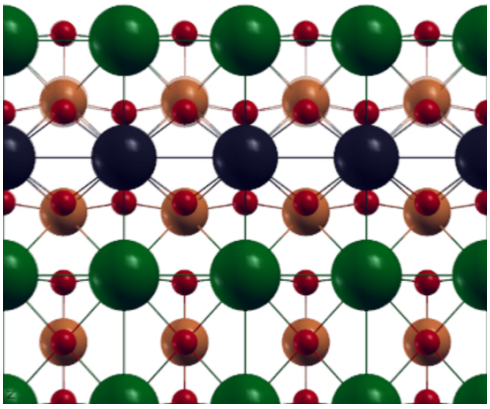

Figure 4.2: Side view of the optimised $BaO(CuO_2)$ surface structure. The blurring illustrates changes compared to the YBCO bulk, for this surface, the largest change appears for the CuO_2 plane that is closer to the top BaO plane compared to the same distance in the bulk.

4.2.2 Surface energies

The optimised YBCO surface slabs consist of two YBCO unit cells. Since the surface and bottom layers are different in each slab, the calculated relaxed energies cannot directly be compared because both the surface energy of the top and the fixed bottom layers affect the energy value. Again, looking in Table 4.1, it can be seen that three of the slabs are mirrored for slabs with multiples of six atomic layers: The mirrored surface slabs are the CuO(BaO) and $BaO(CuO_2)$, the CuO_2(Y) and BaO(CuO), and the Y(CuO_2) and CuO_2(BaO) terminated surfaces. Using the method from Ref. [20] described in subsection 3.5.1 of the Methods chapter, the surface energy contribution of each relaxed surface, E^r, can be calculated from the relative slab energies ε_i, and is presented in Table 4.3. The value of the minimised sum $\sum_i \left(\frac{\vec{\varepsilon_i} - (\hat{A}\vec{E})_i}{\vec{\varepsilon_i}} \right)^2$, denoted residual, is also present in the table as reference.

Table 4.3: Weighted slab energies ε and calculated surface energies E^r for the six ideal surface terminations of YBCO with corresponding residual.

Surface termination		Slab energy (J/m^2)				Surface energy (J/m^2)		Residual $\sum_i \left(\frac{\vec{\varepsilon_i} - (\hat{A}\vec{E})_i}{\vec{\varepsilon_i}} \right)^2$
A	B	ε_1	ε_2	ε_3	ε_4	E^r_A	E^r_B	
CuO(BaO)	$BaO(CuO_2)$	2.83	2.74	2.79	2.70	1.33	1.37	$5.01 \cdot 10^{-10}$
CuO_2(Y)	BaO(CuO)	2.07	1.97	1.88	1.79	0.90	0.89	$6.98 \cdot 10^{-9}$
Y(CuO_2)	CuO_2(BaO)	8.11	7.14	7.59	6.62	3.64	3.59	$1.64 \cdot 10^{-9}$

It can be concluded from Table 4.3 that the weighted slab energies $\varepsilon_{2,3}$ follow the same trend as the surface energies E^r, i.e. that the highest slab energy and surface energy is for the last surface pairs, with the Y(CuO_2) surface as the most unstable. The surface energy for each pair is similar to eachother where the surfaces with the highest energies, and thus less probable, are the two surfaces where the CuO_2-Y structure is broken. The results of surface energies in Table 4.3 are in agreement with the arguments of crystal cleavage of the YBCO crystal [23]: The most stable, and probable, surfaces are the mirrored surfaces terminated by CuO_2(Y) and BaO(CuO).

4.3 Interface structure for STO and YBCO systems

Literature on interface terminations of STO and YBCO mainly focuses on YBCO grown onto STO - substrates used for YBCO growth often consists of STO - where YBCO is slightly stretched out to fit the STO unit cell dimensions, here called the YBCO/STO interface. To find literature on interface terminations for the opposite case where STO is grown onto YBCO (STO/YBCO interface), that is of interest in this work, is more difficult to find. Therefor, literature on both the YBCO/STO and the STO/YBCO interface is included in the discussions below, and is summarised in Table 4.1 with the YBCO surface terminations.

4.3.1 YBCO/STO interfaces

A theoretical study of adhesion energies by Ref. [6] of different YBCO/STO interfaces and with different stacking geometry found two main interfaces. From the SrO surface a CuO_2(BaO) stacking is expected and a BaO(CuO_2) stacking for the TiO_2 terminated STO surface. The CuO_2(BaO) stacking means the first grown layer is CuO_2 and the second is BaO. This growth is also reported in Ref. [21]. In both cases, the interface stacking will initially continue the perovskite stacking of STO: The alternating TiO_2 and SrO layers will be replaced with CuO_2 and BaO when YBCO starts to grow onto STO, and from the third layer, YBCO follow its own layer structure.

An important aspect to consider regarding interfaces between two materials is that they tend to be heterostructures, where the atomic layers are mixed close to the interface or that some of the layers have a different composition. This is reported by Ref. [24] where the atomic structure of the YBCO/STO interface was observed with high-angle annular dark field (HAADF) and Negative Cs imaging (NCSI) techniques. With TiO_2 as the top layer of STO, they found two types of YBCO growth sequences starting with BaO: The BaO(CuO_2) and BaO(CuO) growths, also illustrated in Figure 4.3a.

The two YBCO growths were separated by antiphase domains, and Ref. [24] also found two types of defects of the YBCO growth further away from the interface. In the fist case, two additional layers of CuO and BaO were added before the CuO_2 layer as shown in Figure 4.3b. In the second case, one CuO layer and one BaO layer disappeared compared to the ideal YBCO structure, resulting in the remaining BaO layer being surrounded by two CuO_2 planes, see Figure 4.3c. The changed stacking is a consequence for the antiphase domains and misfit dislocations from the two different YBCO growths. When the layer of YBCO is thick enough, YBCO is no longer affected by the STO substrate, and above the additional or missing CuO and BaO layers, there is a uniform YBCO growth without antiphase domains.

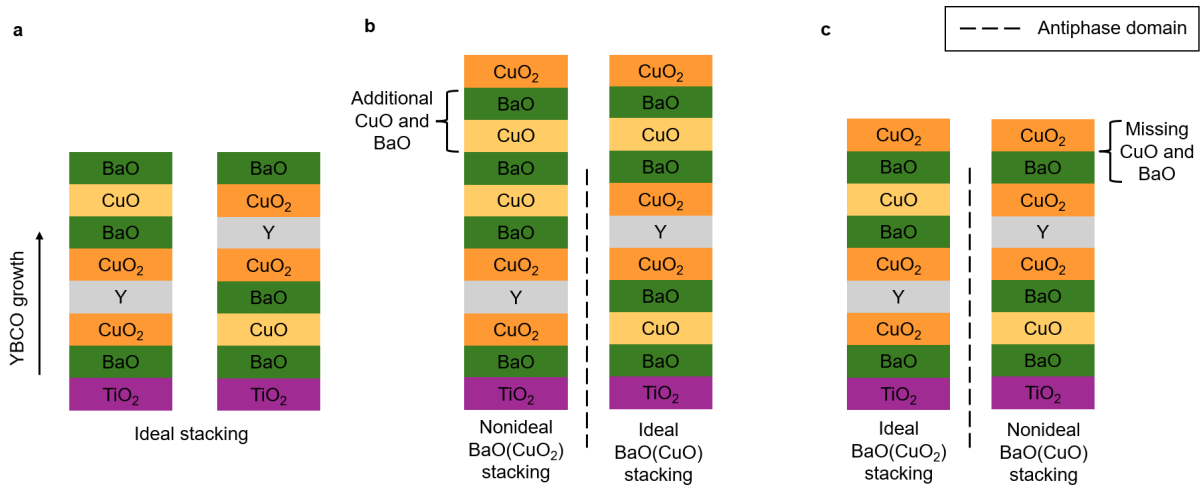

Figure 4.3: Schematic visualisation of the YBCO stacking described in Ref. [24]. Ideal stacking (**a**) and antiphase domains between $BaO(CuO_2)$ and BaO(CuO) stacking compensated in YBCO bulk with (**b**) two additional CuO and BaO layers and (**c**) disappearance of two CuO and BaO layers.

4.3.2 STO/YBCO interfaces

However, the system of interest in this work is a thin film of STO put onto a thick layer of YBCO. Therefore, the STO layers will be compressed in the a and b directions compared to the YBCO unit cell. One previous work, Ref. [21], has from a TEM image of a STO/YBCO/STO interface observed a similar stacking as Ref. [6]: A TiO_2 terminated STO surface with BaO as the first YBCO layer. At the top of the thick YBCO layer there is also a BaO layer and the first grown STO layer is TiO_2. Interesting to add to the discussion is that Ref. [21] claimed that the surface termination of YBCO is CuO(BaO) which does not agree with the their result with a $TiO_2/BaO(CuO_2)$ interface. The phenomena is explained with desorption of the top CuO chain when STO is deposited onto the YBCO surface.

4.3.3 Optimised STO/YBCO interfaces

From the discussion above about both surface terminations of YBCO and and interface structures of YBCO and STO there is no direct link: The YBCO surface do not necessary correspond to the top YBCO layer in a STO/YBCO interface. The lack of literature on STO/YBCO interfaces also makes it hard to make a qualified choice of which interfaces to proceed with for the calculations. This is why the literature review of the opposite YBCO/STO interfaces are included in the results.

Going back to Table 4.1 where the surface and interface terminations are summarised, the $BaO(CuO_2)$ surface would be a promising YBCO surface for a YBCO/STO interface. This YBCO surface is also the only studied for a STO/YBCO interface according the literature review above. The $BaO(CuO_2)$ terminated YBCO surface is thus optimised with both TiO_2 and SrO as the first STO layer. The STO thickness is one unit cell. The interface structures are shown in side view in Figure 4.4. A third interface symbolising that the YBCO surface CuO layer not is destroyed, in contrast to the analysis of the results in Ref. [21], is included in Figure 4.4c with SrO as the first STO layer onto the CuO(BaO) surface. Still with two unit cells of YBCO and one unit cell of STO.

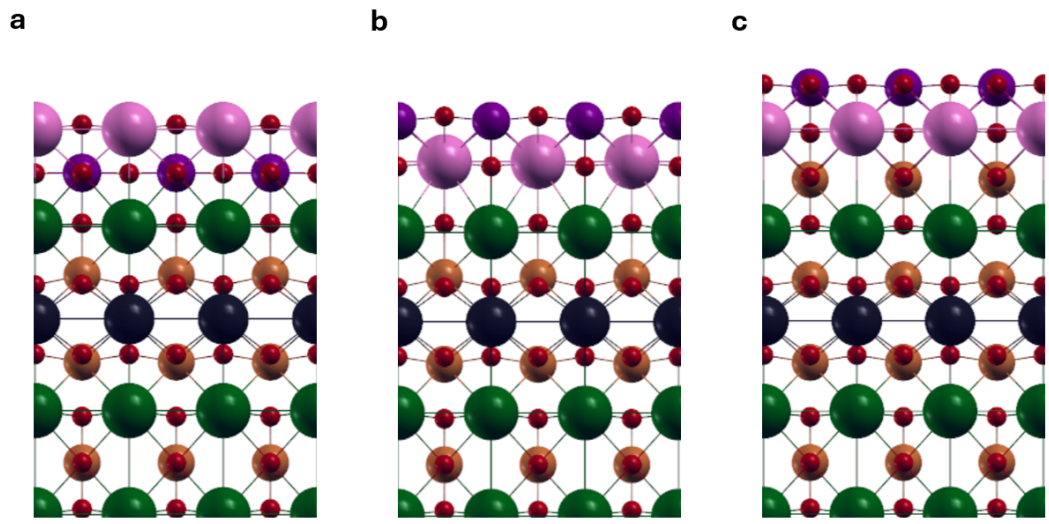

Figure 4.4: Interface geometry viewed in the ac plane of different YBCO surfaces covered with one unit cell of STO: (**a**) The TiO_2/BaO(CuO_2) interface, (**b**) the SrO/BaO(CuO_2) interface and (**c**) the SrO/CuO(BaO) interface.

4.3.4 Atomic distances in the STO/YBCO interface slabs

Similar to the YBCO surfaces, the atomic distances of YBCO in the interface structures are measured to compare the atomic positions with bulk structure. This is presented in Table 4.4. The values for uncapped YBCO are repeated from Table 4.2. First, looking at the TiO_2/BaO(CuO_2) interface, the atomic positions of the two upper YBCO layers are more bulk-like compared to the uncapped surface (3.35 Å and 3.24 Å for capped versus 3.29 Å and 3.25 Å for uncapped BaO(CuO_2) surface). If the first STO layer is SrO instead of TiO_2, there is a larger distance between YBCO and STO, 3.27 Å which is 2.4 % smaller than the bulk distance. The second surface, CuO(BaO) with SrO as first STO layer has YBCO atomic positions very close to bulk, a relative difference of less than 0.5 %, even for the outermost layers which not is the case for the uncapped CuO(BaO) surface.

Table 4.4: Atomic distance (Å) and relative change compared to corresponding bulk value between neighboring YBCO atoms for the three studied interfaces. Values for the corresponding uncapped YBCO surfaces from Table 4.2 is also included.

	Uncapped surface		Surface capped with one unit cell STO		
Atomic distance	CuO (BaO)	BaO (CuO_2)	TiO_2 BaO(CuO_2)	SrO BaO(CuO_2)	SrO CuO(BaO)
Cu-Ba	3.35 (-2.3%)				3.43 (+0.2%)
Ba-Cu	3.37 (+0.5%)	3.29 (-2.0%)	3.35 (+0.0%)	3.27 (-2.4%)	3.36 (+0.1%)
Cu-Y	3.20 (-0.2%)	3.25 (+1.6%)	3.24 (+1.1%)	3.26 (+1.9%)	3.19 (-0.3%)
Y-Cu	3.20 (+0.0%)	3.20 (+0.1%)	3.22 (+0.6%)	3.21 (+0.4%)	3.20 (+0.0%)
Cu-Ba	3.36 (+0.1%)	3.36 (+0.1%)	3.35 (-0.1%)	3.36 (+0.1%)	3.36 (+0.2%)
Ba-Cu	3.43 (+0.1%)	3.43 (+0.1%)	3.43 (+0.2%)	3.43 (+0.1%)	3.43 (+0.1%)
Cu-Ba		3.43 (+0.0%)	3.43 (+0.0%)	3.43 (+0.0%)	

4.4 Difference in electron density

The TiO_2/BaO interface is further investigated to analyse how the thickness of the STO capping layer affects the electron density. Onto the YBCO surface, STO of 1, 1.5, 2.5 and 3.5 unit cells are added. The difference in electron density $\Delta n(r)$, defined in Eq. (3.5) of the Methods chapter, is shown in Figure 4.5 for the center plane and outer plane of the interface slabs. Atoms in respective cross section are also present. Atomic YBCO layers below the Y plane of YBCO did not show any charge redistribution and is therefore excluded in Figure 4.5. The color scheme of $\Delta n(r)$ represents electrons moving from blue to red regions, for the total system compared to the separated. Stronger colors represent larger differences.

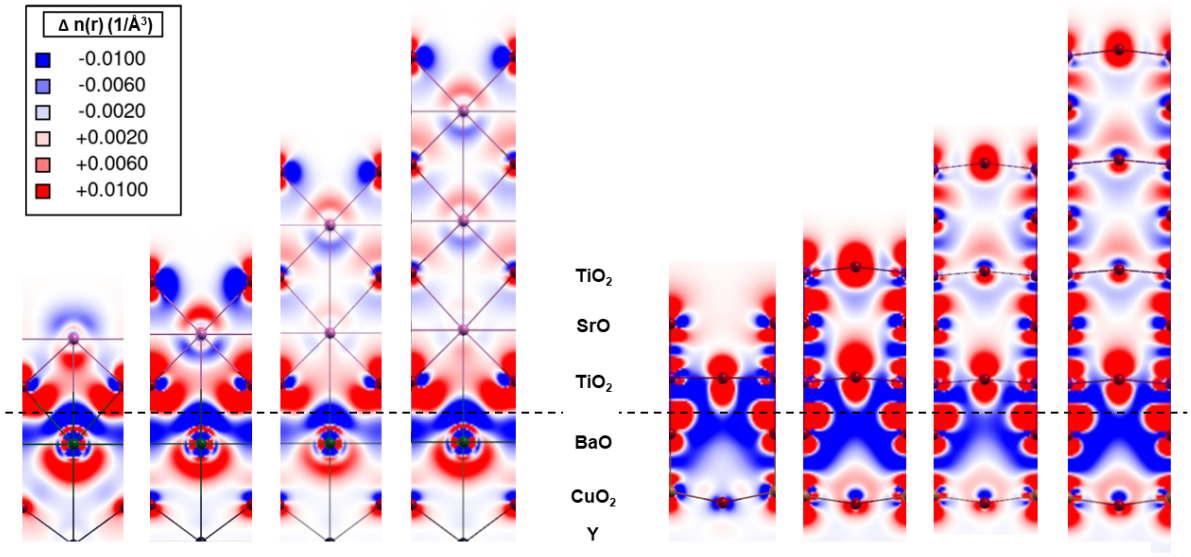

Figure 4.5: Difference in electron density $\Delta n(r)$ for the TiO_2/BaO(CuO_2) interface with 1, 1.5, 2.5 and 3.5 STO unit cells. Cross section of the center plane (left) and outer plane (right) through the unit slab in side view. The dashed line represents the interface.

A clear shift of charge distribution is seen at the interface (dashed line in Figure 4.5) where electrons that were at the surfaces for the separated systems move to the closest atoms for the STO/YBCO interface, independent of the STO thickness. The change is most noticeable around the O atoms, both in the top BaO layer and the first STO atomic layer, TiO_2. This conclusion is in agreement with the interface structure of YBCO/STO studied in Ref. [6]. Even if the lattice parameters are slightly different, the electron density differences are comparable.

The plot of differences in electron density tells something about how STO capping can protect YBCO surfaces. Ref. [6] reports that the charge distribution between the outermost Ti and O from the BaO layer, is very similar to Ti-O in STO bulk and that O atoms at the interface tend to belong to the TiO_2 layer of the interface. Figure 4.5 also indicates, independent of the STO capping thickness, that the TiO_2/BaO interface shows same redistribution of charge. That means, adding STO on YBCO extends the YBCO film with a buffer layer where YBCO even at the interface becomes bulk-like and no longer has the surface properties and the risk to react with the environment and thus loose the superconducting properties.

Comparing the interfaces ending with TiO_2, it can be seen that the interface capped with 1.5

unit cell of STO shows a larger movement of electron density compared to thicker capping. This indicates that charge is transported between both STO surfaces for a thin capping. As the thickness of the STO film increases, STO becomes more bulk-like, and $\Delta n(r)$ between the STO surfaces do not affect each other to an equal extent. For instance, the second STO atomic layer, SrO, shows same $\Delta n(r)$ behaviour for 2.5 and 3.5 STO unit cells, and the main difference between these capping thicknesses is nothing but the capping thickness. This should be compared with 1.5 STO capping, where there is a large charge transport around Sr in the SrO layer. Still, the top STO layer shows a charge redistribution, meaning the capping is not thick enough for STO to be completely bulk-like at its surface, as YBCO is below the third, Y ion layer.

Corresponding analysis of interfaces with the SrO surfaces was not made, due to the time limit of this project. However, for the TiO_2/BaO interface, it would be interesting to analyse the $\Delta n(r)$ plot of 2 and 3 STO unit cells as well, to get a comprehensive analysis of the electron density STO capping dependence for the TiO_2/BaO(CuO_2) interface. Despite that, the analysis of $\Delta n(r)$ shows that the similar lattice structure of STO capping has an effect on the charge distribution of YBCO.

5
Conclusion and outlook

The results in this project determined the $YBa_2Cu_3O_7$ (YBCO) surfaces terminated by CuO_2(Y) and BaO(CuO) as the most stable, in agreement with bond strength between the layers in YBCO. The method of determining the surface energy of a slab consequently work well for YBCO slabs of twelve atomic layers. However, the literature review shows that experimentally determined YBCO surfaces show a larger variation, also with different surface termination for same sample.

Interface structures on the other hand cannot be directly related to uncapped YBCO surfaces. Other top YBCO layers at the interfaces with $SrTiO_3$ (STO) and YBCO are found than clean YBCO surfaces, because of surface reactions of YBCO. Studying the optimised interface structures, it can be seen that, depending on how STO is grown, it is possible to make the YBCO atomic positions more similar to bulk, than without capping, which is a promising effect of STO capping. The analysis of difference in electron density shows that charges are redistributed around the STO/YBCO interface. Possibly, this can indicate that even a atomic thin film of STO can conserve the superconducting properties of YBCO. Even if the scope of this thesis is too small to draw definite conclusions, this hints to interesting future work.

The accuracy of the density functional theory (DFT) calculations in this project is limited by convergence thresholds, number of k points and other input data. Despite that, the results of the calculations still are valuable, even if a further improvement would be to increase the threshold values, with longer computation time. Early in the project, it was also seen that the choice of pseudopotentials affected whether the calculated system converged and it would be interesting to further investigate the PBEsol-potentials for YBCO and STO systems.

This work is limited to calculations, but the calculations were made to resemble the dimensions of the STO/YBCO systems presented by Ref. [11]. To better understand the physical system from a theoretical perspective, even non-ideal structures have to be considered throughout the calculations. More important than to improve the results, is to proceed the analysis of difference in electron densities for STO/YBCO systems, since only one interface was analysed in that way. Calculations on more interfaces as well as experimental research on STO/YBCO interface terminations are also keys to knowing more about how STO capping affects the properties of YBCO surfaces.

Bibliography

[1] K. M. Shen and J. C. S. Davis. "Cuprate high-Tc superconductors". In: *Materials Today* 11.9 (2008), pp. 14–21. ISSN: 1369-7021. DOI: https://doi.org/10.1016/S1369-7021(08)70175-5.

[2] M. K. Wu, J. R. Ashburn, C. J. Torng, et al. "Superconductivity at 93 K in a new mixed-phase Y-Ba-Cu-O compound system at ambient pressure". In: *Phys. Rev. Lett.* 58 (9 Mar. 1987), pp. 908–910. DOI: https://link.aps.org/doi/10.1103/PhysRevLett.58.908.

[3] H. Iwasawa, N. B. M. Schröter, T. Masui, et al. "Surface termination and electronic reconstruction in $YBa_2Cu_3O_{7-\delta}$". In: *Phys. Rev. B* 98 (8 Aug. 2018), p. 081112. DOI: https://link.aps.org/doi/10.1103/PhysRevB.98.081112.

[4] A. Godeke. "High temperature superconductors for commercial magnets". In: *Superconductor Science and Technology* 36.11 (Oct. 2023), p. 113001. DOI: https://dx.doi.org/10.1088/1361-6668/acf901.

[5] A. Jain, S. P. Ong, G. Hautier, et al. "Commentary: The Materials Project: A materials genome approach to accelerating materials innovation". In: *APL Materials* 1.1 (July 2013), p. 011002. ISSN: 2166-532X. DOI: https://doi.org/10.1063/1.4812323.

[6] Z. Wang, S. Tsukimoto, M. Saito, et al. "Atomic and electronic structure of the $YBa_2Cu_3O_7$/$SrTiO_3$ interface from first principles". In: *Journal of Applied Physics* 106.9 (Nov. 2009), p. 093714. ISSN: 0021-8979. DOI: https://doi.org/10.1063/1.3257264.

[7] M. F. Yan, R. L. Barns, H. M. O'Bryan Jr, et al. "Water interaction with the superconducting YBa2Cu3O7 phase". In: *Applied Physics Letters* 51.7 (Aug. 1987), pp. 532–534. ISSN: 0003-6951. DOI: https://doi.org/10.1063/1.98389.

[8] I. von Lampe, F. Zygalsky, H. Nagibzadeh, et al. "Influence of cation modification on the environmental degradation of high temperature superconducting Y–Ba–Cu–O films". In: *Physica C: Superconductivity* 436.2 (2006), pp. 123–127. ISSN: 0921-4534. DOI: https://doi.org/10.1016/j.physc.2006.02.010.

[9] Q. Ran, Z. Jing, L. Shen, et al. "Suppression of flux avalanches in YBCO superconducting thin films by coating metal investigated using magneto-optical imaging". In: *Superconductivity* 11 (2024), p. 100101. ISSN: 2772-8307. DOI: https://doi.org/10.1016/j.supcon.2024.100101.

[10] B. R. David, D. Grundler, R. Eckart, et al. "A multi-layer process for the fabrication of HTSC flux transformers and SQUIDS". In: *Superconductor Science and Technology* 7.5 (May 1994), p. 287. DOI: https://dx.doi.org/10.1088/0953-2048/7/5/015.

[11] A. Kalaboukhov. "YBCO surface passivation". Unpublished. 2023.

[12] W. Koch and M. C. Holthausen. *A Chemists Guide to Density Functional Theory*. 2nd ed. Wiley-VCH, Weinheim, 2001. ISBN: 978-3-527-30372-4.

[13] P. Giannozzi, S. Baroni, N. Bonini, et al. “QUANTUM ESPRESSO: a modular and open-source software project for quantum simulations of materials”. In: *Journal of Physics: Condensed Matter* 21.39 (Sept. 2009), p. 395502. DOI: https://dx.doi.org/10.1088/0953-8984/21/39/395502.

[14] P. Giannozzi, O. Andreussi, T. Brumme, et al. “Advanced capabilities for materials modelling with Quantum ESPRESSO”. In: *Journal of Physics: Condensed Matter* 29.46 (Oct. 2017), p. 465901. DOI: https://dx.doi.org/10.1088/1361-648X/aa8f79.

[15] P. Giannozzi, O. Baseggio, P. Bonfà, et al. “Quantum ESPRESSO toward the exascale”. In: *The Journal of Chemical Physics* 152.15 (Apr. 2020), p. 154105. ISSN: 0021-9606. DOI: https://doi.org/10.1063/5.0005082. URL: http://www.quantum-espresso.org.

[16] A. Kokalj. “XCrySDen—a new program for displaying crystalline structures and electron densities”. In: *Journal of Molecular Graphics and Modelling* 17.3 (1999), pp. 176–179. ISSN: 1093-3263. DOI: https://doi.org/10.1016/S1093-3263(99)00028-5.

[17] M. Dion, H. Rydberg, E. Schröder, et al. “Van der Waals Density Functional for General Geometries”. In: *Phys. Rev. Lett.* 92 (24 June 2004), p. 246401. DOI: https://link.aps.org/doi/10.1103/PhysRevLett.92.246401.

[18] K. Berland and P. Hyldgaard. “Exchange functional that tests the robustness of the plasmon description of the van der Waals density functional”. In: *Phys. Rev. B* 89 (3 Jan. 2014), p. 035412. DOI: https://link.aps.org/doi/10.1103/PhysRevB.89.035412.

[19] A. Dal Corso. “Pseudopotentials periodic table: From H to Pu”. In: *Computational Materials Science* 95 (2014), pp. 337–350. ISSN: 0927-0256. DOI: https://doi.org/10.1016/j.commatsci.2014.07.043.

[20] N. M. Stuart and K. Sohlberg. “A method of calculating surface energies for asymmetric slab models”. In: *Phys. Chem. Chem. Phys.* 25 (19 2023), pp. 13351–13358. DOI: http://dx.doi.org/10.1039/D2CP04460A.

[21] T. Gagnidze. “Investigation of electronic structure at the $SrTiO_3$/$YBa_2Cu_3O_7$ interface”. PhD thesis. ETH Zürich, 2019.

[22] G. Frank, Ch. Ziegler, and W. Göpel. “Surface composition of clean, epitaxial thin films of $YBa_2Cu_3O_{7-x}$ from quantitative x-ray photoemission spectroscopy analysis”. In: *Phys. Rev. B* 43 (4 Feb. 1991), pp. 2828–2834. DOI: https://link.aps.org/doi/10.1103/PhysRevB.43.2828.

[23] C. Calandra and F. Manghi. “Surface termination of $YBa_2Cu_3O_{7-x}$ systems”. In: *Journal of Electron Spectroscopy and Related Phenomena* 66.3 (1994), pp. 453–467. ISSN: 0368-2048. DOI: https://doi.org/10.1016/0368-2048(93)01852-6.

[24] S.B. Mi. “Interfacial defects in $YBa_2Cu_3O_{7-\delta}$/$SrTiO_3$(001) heterostructures studied by aberration-corrected ultrahigh-resolution electron microscopy”. In: *Philosophical Magazine Letters* 93.5 (2013), pp. 264–272. DOI: https://doi.org/10.1080/09500839.2013.765975.

DEPARTMENT OF MICROTECHNOLOGY AND NANOSCIENCE (MC2)
CHALMERS UNIVERSITY OF TECHNOLOGY
Gothenburg, Sweden
www.chalmers.se

CHALMERS
UNIVERSITY OF TECHNOLOGY